Available online at www.sciencedirect.com
SCIENCE DIRECT®
Control Engineering Practice 14 (2006) 277–293
CONTROL ENGINEERING PRACTICE
www.elsevier.com/locate/conengprac

Control-oriented model of fuel processor for hydrogen generation in fuel cell applications

Jay Pukrushpan[a,*], Anna Stefanopoulou[b], Subbarao Varigonda[c], Jonas Eborn[c], Christoph Haugstetter[c]

[a]Department of Mechanical Engineering, Kasetsart University, Bangkok, 10900 Thailand
[b]Department of Mechanical Engineering, University of Michigan, Ann Arbor, MI, USA
[c]United Technologies Research Center, East Hartford, CT, USA

Received 26 October 2004; accepted 8 April 2005
Available online 29 June 2005

Abstract

A control-oriented dynamic model of a catalytic partial oxidation-based fuel processor is developed using physics-based principles. The fuel processor system (FPS) converts a hydrocarbon fuel to a hydrogen (H_2)-rich mixture that is directly feed to the proton exchange membrane fuel cell stack (PEM-FCS). Cost and performance requirements of the total powerplant typically lead to highly integrated designs and stringent control objectives. Physics-based component models are extremely useful in understanding the system level interactions, implications on system performance and in model-based controller design. The model can be used in a multivariable analysis to determine characteristics of the system that might limit performance of a controller or a control design.

In this paper, control theoretic tools such as the relative gain array (RGA) and the observability gramian are employed to guide the control design for a FPS combined with a PEM-FC. For example, this simple multivariable analysis suggests that a decrease in hydro-desulfurizer volume is critical for the H_2-starvation control. Moreover, RGA analysis shows different level of coupling between the system dynamics at different power levels. Finally, the observability analysis can help in assessing the relative cost–benefit ratio in adding extra sensors in the system.

Keywords: Fuel processor; Fuel cell; Hydrogen generation; Catalytic partial oxidation; Multivariable analysis

1. Introduction

Inadequate infrastructure for hydrogen (H_2) refueling, distribution, and storage makes fuel processor technology an important part of the fuel cell system. Methanol, gasoline, and natural gas are examples of fuels being considered as fuel cell energy sources. Fig. 1 illustrates different processes involved in converting carbon-based fuel to H_2 (Birch, 2001; Brown, 2001).

For residential applications, fueling the fuel cell system using natural gas is often preferred because of its wide availability and extended distribution system (Dicks, 1996). Common methods of converting natural gas to H_2 include steam reforming and partial oxidation (POX). The most common method, steam reforming, which is endothermic, is well suited for steady-state operation and can deliver a relatively high concentration of H_2 (Ahmed & Krumpelt, 2001), but it suffers from a poor transient operation (Brown, 2001). On the other hand, the POX offers several other advantages such as compactness, rapid-startup, and responsiveness to load changes (Dicks, 1996), but delivers lower conversion efficiency.

The main reactor of a POX-based natural gas fuel processing system (FPS) is a catalytic POX (CPOX) reactor. Here, H_2-rich gas is produced by mixing natural

*Corresponding author. Tel.: +66 29428555x1834; fax: +66 25794576.
E-mail address: fengjwp@ku.ac.th (J. Pukrushpan).

0967-0661/$ - see front matter © 2005 Elsevier Ltd. All rights reserved.
doi:10.1016/j.conengprac.2005.04.014

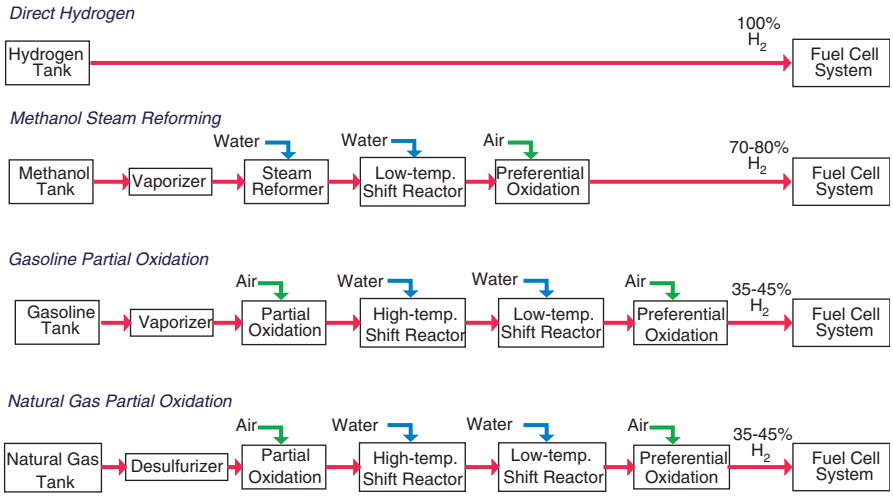

Fig. 1. Fuel sources for fuel cell systems (Birch, 2001; Brown, 2001).

gas with air over a catalyst bed. The amount of H_2 created in the FPS depends on both the catalyst bed temperature and the CPOX air-to-fuel ratio, more specifically, the oxygen-to-carbon ratio (O2C). This O2C ratio also influences the amount of heat generated in the CPOX, which then affects the CPOX catalyst bed temperature.

System level dynamic models of fuel cell power plants built from physics-based component models are extremely useful in understanding the system level interactions, implications for system performance and model-aided controller design. The system level dynamic models also help in evaluating alternative system architectures in an integrated design and control paradigm. In this paper, we develop a dynamic model for the FPS control of the air blower and the fuel valve for fast and efficient H_2 generation. More specifically, we concentrate on the dynamics associated with two main control objectives. First, to prevent stack H_2 starvation, which can permanently damage the stack (Song, Kim, & Shin, 2000; Yang, Bates, Fletcher, &Pow,), the H_2 flow from the FPS must respond rapidly and robustly to changes in stack power level, i.e. changes in stack current (Pukrushpan, Stefanopoulou, & Peng, 2004). Unfortunately, oversupply of H_2 by adjusting the FPS flow at a higher steady-state level is not an option because this will cause wasted H_2 from the anode exhaust (Song et al., 2000). Thus, H_2 generation needs to follow the current load in a precise and fast manner. Second, the temperature of the CPOX must be maintained at a certain point. Exposure to high temperature will permanently damage the CPOX catalyst bed while low CPOX temperature slows down the fuel reaction rate (Zhu, Zhang, & King, 2001). The optimization of these goals during transient operations can be achieved by coordinating CPOX air blower command and the fuel (natural gas) valve command.

We neglect variations of the pressure, concentration and temperature within various system stages and lump them into spatially averaged variables and can be described using ordinary differential equations. The model is parameterized and validated against the results from a high-order fuel cell system model (Eborn, Pedersen, Haugstetter, & Ghosh, 2003).

Two applications of the model are then presented. Specifically, we demonstrate how control theoretic tools can be used to analyze necessary tradeoffs between the two control objectives, and thus, guide the controller and system design. First, the relative gain array (RGA) analysis is applied to the model to determine control input/output pairs and to identify the interactions between two control loops. Moreover, we demonstrate how simple linear observability analysis can facilitate decisions on sensor selection.

2. Overview of the fuel processing system

Fig. 2 illustrates the components in a natural gas FPS (Thomas, James, Lomax, & Kuhn, 2000). The FPS is composed of four main reactors, namely, hydro-desulfurizer (HDS), CPOX, water–gas shift (WGS), and preferential oxidation (PROX). Natural gas (Methane CH_4) is supplied to the FPS from either a high-pressure tank or a high-pressure pipeline. Sulfur, which poisons the WGS catalyst (Brown, 2001), is then removed from the natural gas stream in the HDS (Dicks, 1996; Gardner, Berry, Lyons, Beer, & Freed, 2002). The main air flow is supplied to the system by a blower (BLO) which draws air from the atmosphere. The air is then heated in the heat exchanger (HEX). The heated air and the de-sulfurized natural gas stream are then mixed in the mixer (MIX). The mixture is then passed through the catalyst bed inside the catalytic

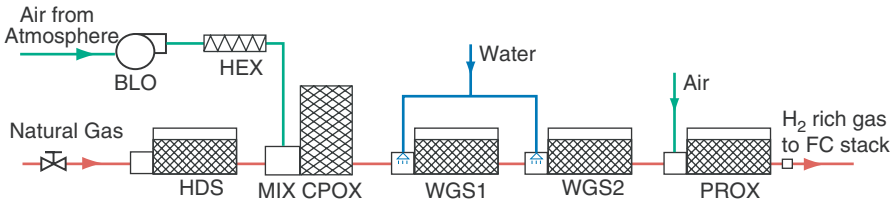

Fig. 2. FPS components.

partial oxidizer (CPOX), where CH_4 reacts with oxygen to produce H_2. There are two main chemical reactions taking place in the CPOX: POX and total oxidation (TOX) (Larentis, de Resende, Salim, & Pinto, 2001; Zhu et al., 2001):

$$(POX) \quad CH_4 + \tfrac{1}{2}O_2 \rightarrow CO + 2H_2, \tag{1}$$

$$(TOX) \quad CH_4 + 2O_2 \rightarrow CO_2 + 2H_2O. \tag{2}$$

Heat is released from both reactions. However, TOX reaction releases more heat than POX reaction. The difference in the rates of the two reactions depends on the selectivity, S, defined as

$$S = \frac{\text{Rate of } CH_4 \text{ reacting in POX}}{\text{Total rate of } CH_4 \text{ reacting}}. \tag{3}$$

The selectivity depends strongly on the O2C (O_2-to-CH_4) ratio entering the CPOX (Zhu et al., 2001). H_2 is created only in POX reaction and, therefore, it is preferable to promote this reaction in the CPOX. However, carbon monoxide (CO) is also created along with H_2 in the POX reaction as can be seen in (1). Since CO poisons the fuel cell catalyst, it is eliminated using both the WGS converter and the preferential oxidizer (PROX). As illustrated in Fig. 2, there are typically two WGS reactors operating at different temperatures (Brown, 2001; Ledjeff-Hey, Roses, & Wolters, 2000). In the WGS, water is injected into the gas flow in order to promote a WGS reaction

$$(WGS) \quad CO + H_2O \rightarrow CO_2 + H_2. \tag{4}$$

Note that even though the objective of WGS is to eliminate CO, H_2 is also created from the WGS reaction. The level of CO in the gas stream after WGS is normally still high for fuel cell operation and thus oxygen is injected (in the form of air) into the PROX reactor to react with the remaining CO

$$(PROX) \quad 2CO + O_2 \rightarrow 2CO_2. \tag{5}$$

The amount of air injected into the PROX is typically twice the amount that is needed to maintain the stoichiometric reaction in (5) (Brown, 2001; Doss, Kumar, Ahluwalia, & Krumpelt, 2001).

3. Control-oriented FPS model

The FPS model is developed with a focus on the dynamic behaviors associated with the flows and pressures in the FPS and also the temperature of the CPOX. The dynamic model is used to study the effects of fuel and air flow command to (i) CPOX temperature (Zhu et al., 2001), (ii) stack H_2 concentration (Song et al., 2000), and (iii) steady-state stack efficiency. The stack efficiency is interpreted as the H_2 utilization, which is the ratio between the H_2 reacted in the fuel cell stack and the amount of H_2 supplied to the stack.

3.1. Modeling assumptions

Several assumptions are made in order to simplify the FPS model. Since the control of WGS and PROX reactants are not studied, the two components are lumped together as one volume and the combined volume is called WROX (WGS + PROX). It is also assumed that both components are perfectly controlled such that the desired values of the reactants are supplied to the reactors. Furthermore, because the amount of H_2 created in WGS is proportional to the amount of CO that reacts in WGS (Reaction (4)), which in turn, is proportional to the amount of H_2 generated in CPOX (Reaction (1)), it is assumed that the amount of H_2 generated in the WGS is always a fixed percentage of the amount of H_2 produced in the CPOX. The desulfurization process in the HDS is not modeled and thus the HDS is viewed as a storage volume. It is assumed that the composition of the air entering the blower is constant. Additionally, any temperature other than the CPOX temperature is assumed constant and the effect of temperature changes on the pressure dynamics is assumed negligible. The volume of CPOX is relatively small and is thus ignored. It is also assumed that the CPOX reaction is rapid and reaches equilibrium before the flow exit the CPOX reactor. Finally, all gases obey the ideal gas law and all gas mixtures are perfect mixtures. Fig. 3 illustrates the simplified system and state variables used in the model. The physical constants used throughout the model are given in Table 1 and the properties of the air entering the blower (approximately 40% relative humidity) are given in Table 2.

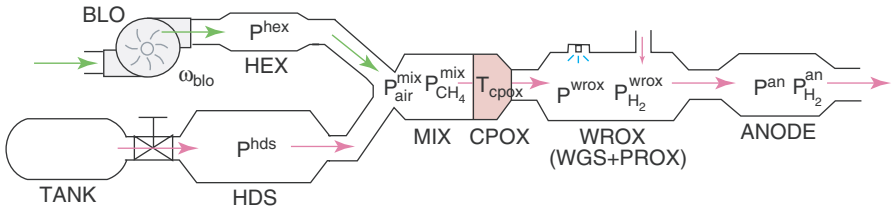

Fig. 3. FPS dynamic model.

Table 1
Physical constants

Parameter	Value
R	8.3145 J/mol K
M_{N_2}	28×10^{-3} kg/mol
M_{CH_4}	16×10^{-3} kg/mol
M_{CO}	28×10^{-3} kg/mol
M_{CO_2}	44×10^{-3} kg/mol
M_{H_2}	2×10^{-3} kg/mol
M_{H_2O}	18×10^{-3} kg/mol
M_{O_2}	32×10^{-3} kg/mol
F	96 485 C

Table 2
Conditions of the atmospheric air entering the blower

Parameter	Value
p_{amb}	1×10^5 Pa
$y^{atm}_{N_2}$	0.6873
$y^{atm}_{H_2O}$	0.13
$y^{atm}_{O_2}$	0.1827
M^{atm}_{air}	27.4×10^{-3} kg/mol

3.2. Model states and principles

The dynamic states in the model, shown also in Fig. 3, are blower speed, ω_{blo}, heat exchanger pressure, p^{hex}, HDS pressure, p^{hds}, mixer CH_4 partial pressure, $p^{mix}_{CH_4}$, mixer air partial pressure, p^{mix}_{air}, CPOX temperature, T_{cpox}, WROX (combined WGS and PROX) volume pressure, p^{wrox}, WROX H_2 partial pressure, $p^{wrox}_{H_2}$, anode pressure, p^{an}, and anode H_2 partial pressure, $p^{an}_{H_2}$. Mass conservation with the ideal gas law through the isothermal assumption is used to model the filling dynamics of the gas in all volumes considered in the system. The orifice equation with a turbulent flow assumption is used to calculate flow rates between two volumes. The energy conservation principle is used to model the changes in CPOX temperature. The conversion of the gases in CPOX is based on the reactions in (1) and (2) and the selectivity defined in (3).

3.3. Orifice

The flow between any two volumes in the FPS system is based on the orifice flow equation. Specifically, the mass flow rate between two volumes is given as a function of upstream pressure, p_1, and downstream pressure, p_2. The flow is assumed turbulent and the rate is governed by

$$W = W_0 \sqrt{\frac{p_1 - p_2}{\Delta p_0}}, \tag{6}$$

where W_0 and Δp_0 are the nominal air flow rate and the nominal pressure drop of the orifice, respectively.

3.4. Blower

The speed of the blower is modeled as a first-order dynamic system with time constant τ_b. The governing equation is

$$\frac{d\omega_{blo}}{dt} = \frac{1}{\tau_b}\left(\frac{u_{blo}}{100}\omega_0 - \omega_{blo}\right), \tag{7}$$

where u_{blo} is the blower command signal (range between 0 and 100) and ω_0 is the nominal blower speed (3600 rpm). The gas flow rate through the blower, W_{blo}, is determined using the blower map, which represents the relation between a scaled blower volumetric flow rate and a scaled pressure head (Boyce, 1982). The scaled pressure head is the actual pressure head scaled by a square of the speed ratio, i.e. [scaled pressure head] = [actual head] $(\omega/\omega_0)^2$ and the scaled volumetric flow rate is the actual flow rate scaled by the reciprocal of the speed ratio, i.e.,

$$[\text{scaled flow}] = \frac{[\text{actual flow}]}{(\omega/\omega_0)}.$$

Note that the changes in gas density are ignored and thus only the blower speed is used in the scaling. The blower mass flow rate, W_{blo}, is calculated by multiplying the volumetric flow rate with constant air density ($1.13\,kg/m^3$). The blower time constant is 0.3 s.

3.5. Heat exchanger volume

The only dynamics considered in the heat exchanger is the pressure dynamics. The changes in temperature of

the gas are ignored and it is assumed that the effects of actual temperature changes on the pressure dynamics are negligible. The rate of change in air pressure of the HEX is described by

$$\frac{dp^{hex}}{dt} = \frac{RT_{hex}}{M_{air}^{atm} V_{hex}} (W^{blo} - W^{hex}), \tag{8}$$

where M_{air}^{atm} is the molecular weight of the air flow through the blower (given in Table 2). The orifice flow (6) is used to calculate the outlet flow rate of the HEX, W^{hex}, as a function of HEX pressure, p^{hex}, and mixer pressure, p^{mix}.

3.6. Hydro-desulfurizer volume

The pressure of the gas in the HDS is governed by the mass balance principle. It is assumed that the natural gas fed to the HDS is pure CH_4 (Brown, 2001), and thus the desulfurization process is not modeled. The HDS is then considered as a gas volume and the pressure changes are modeled by

$$\frac{dp^{hds}}{dt} = \frac{RT_{hds}}{M_{CH_4} V_{hds}} (W_{fuel} - W^{hds}), \tag{9}$$

where W^{hds} is the rate of mass flow from HDS to the mixer (MIX), and is calculated as a function of p^{hds} and p^{mix} using the orifice (6). The temperature of the gas, T_{hds}, is assumed constant.

The flow rate of CH_4 into the HDS, W_{fuel}, is controlled by a fuel valve. The orifice (6) with variable gain based on the valve input signal, u_{valve} (0–100), is used to model the flow through the valve.

$$W_{fuel} = \left(\frac{u_{valve}}{100}\right) W_{0,valve} \sqrt{\frac{p^{tank} - p^{hds}}{\Delta p_{0,valve}}}, \tag{10}$$

where p^{tank} is the fuel tank or supply line pressure.

3.7. Mixer

The natural gas flow from the HDS, W^{hds}, and the air flow from the blower, W^{hex}, are combined in the mixer (MIX). Two dynamic variables in the mixer model are the CH_4 pressure, $p_{CH_4}^{mix}$, and the air pressure, p_{air}^{mix}. The state equations of the MIX model are

$$\frac{dp_{CH_4}^{mix}}{dt} = \frac{RT_{mix}}{M_{CH_4} V_{mix}} (W^{hds} - x_{CH_4}^{mix} W^{cpox}), \tag{11}$$

$$\frac{dp_{air}^{mix}}{dt} = \frac{RT_{mix}}{M_{air}^{atm} V_{mix}} (W^{hex} - x_{air}^{mix} W^{cpox}), \tag{12}$$

where W^{cpox} is the flow rate through the CPOX which is calculated in Section 3.8. The mixer total pressure is the sum of the CH_4 and the air pressures, $p^{mix} = p_{CH_4}^{mix} + p_{air}^{mix}$. Based on $p_{CH_4}^{mix}$ and p_{air}^{mix}, the mass fractions of CH_4 and the air in the mixer, $x_{CH_4}^{mix}$ and x_{air}^{mix}, are calculated by

$$x_{CH_4}^{mix} = \frac{1}{1 + (M_{air}^{atm}/M_{CH_4})(p_{air}^{mix}/p_{CH_4}^{mix})}, \tag{13}$$

$$x_{air}^{mix} = \frac{1}{1 + (M_{CH_4}/M_{air}^{atm})(p_{CH_4}^{mix}/p_{air}^{mix})}, \tag{14}$$

where M_{CH_4} and M_{air}^{atm} are the molar masses of CH_4 and atmospheric air, respectively (see Table 2). Note that $x_{CH_4}^{mix} + x_{air}^{mix} = 1$ since the gas in MIX volume is composed of CH_4 and atmospheric air. The temperature of the mixer gas, T_{mix}, is assumed constant.

The mass fractions of nitrogen, oxygen and vapor in the mixer needed for the calculation of the CPOX reactions are calculated by

$$x_{N_2}^{mix} = x_{N_2}^{atm} x_{air}^{mix}, \tag{15}$$

$$x_{O_2}^{mix} = x_{O_2}^{atm} x_{air}^{mix}, \tag{16}$$

$$x_{H_2O}^{mix} = x_{H_2O}^{atm} x_{air}^{mix}, \tag{17}$$

where x_i^{atm} is the mass fraction of species i in atmospheric air, which is calculated from the mass fractions given in Table 2. Note that $x_{N_2}^{mix} + x_{O_2}^{mix} + x_{H_2O}^{mix} = x_{air}^{mix}$. The O2C, i.e., O_2-to-CH_4, (mole) ratio, λ_{O2C}, which influences the reaction rate in the CPOX, is calculated by

$$\lambda_{O2C} \equiv \frac{n_{O_2}}{n_{CH_4}} = y_{O_2}^{atm} \frac{p_{air}^{mix}}{p_{CH_4}^{mix}}, \tag{18}$$

where n_i is the number of moles of species i, and $y_{O_2}^{atm}$ is the oxygen mole fraction of the atmospheric air given in Table 2.

3.8. Catalytic partial oxidation

Since the gas volume in the CPOX catalyst bed is relatively small, the pressure dynamics of the gas is ignored. The flow rate though the CPOX, W^{cpox}, is calculated using the orifice (6) as a function of mixer total pressure, p^{mix}, and the total pressure in WGS and PROX combined volume, p^{wrox}. The only dynamics considered in the CPOX is the catalyst temperature, T_{cpox}. The temperature dynamics is modeled using energy balance equation

$$m_{bed}^{cpox} C_{P,bed}^{cpox} \frac{dT_{cpox}}{dt} = \begin{bmatrix} \text{inlet enthalpy} \\ \text{flow} \end{bmatrix} - \begin{bmatrix} \text{outlet} \\ \text{enthalpy} \\ \text{flow} \end{bmatrix} + \begin{bmatrix} \text{heat} \\ \text{from reactions} \end{bmatrix}, \tag{19}$$

where m_{bed}^{cpox} (kg) and $C_{P,bed}^{cpox}$ (J/kg K) are mass and specific heat capacity of the catalyst bed, respectively. The last two terms on the right-hand side of (19) depend on the reaction taking place in the CPOX.

In the CPOX reactor, CH_4 is oxidized to produce H_2. There are two CH_4 oxidation reactions: POX and TOX.

$$(POX)\quad CH_4 + \tfrac{1}{2}O_2 \rightarrow CO + 2H_2, \tag{20}$$

$$(TOX)\quad CH_4 + 2O_2 \rightarrow CO_2 + 2H_2O. \tag{21}$$

The heat of reaction of POX and TOX reactions are $\Delta H_{pox}^0 = -0.036 \times 10^6$ J/mol of CH_4 and $\Delta H_{tox}^0 = -0.8026 \times 10^6$ J/mol of CH_4, respectively. The other two secondary reactions considered here are water formation, or H_2 oxidation (HOX), and CO preferential oxidation (COX).

$$(HOX)\quad 2H_2 + O_2 \rightarrow 2H_2O, \tag{22}$$

$$(COX)\quad 2CO + O_2 \rightarrow 2CO_2. \tag{23}$$

The heat of reaction of HOX and COX reactions are $\Delta H_{hox}^0 = -0.4836 \times 10^6$ J/mol of O_2 and $\Delta H_{cox}^0 = -0.566 \times 10^6$ J/mol of O_2, respectively. The species entering the CPOX include CH_4, O_2, H_2O, and N_2. Nitrogen does not react in the CPOX. The water may react with CH_4 through steam-reforming reaction (Brown, 2001); however, this reaction is ignored in this study. CH_4 reacts with oxygen to create the final product, which contains H_2, H_2O, CO, CO_2, CH_4, and O_2 (Zhu et al., 2001). The amount of each species depends on the initial O2C (O_2-to-CH_4) ratio, λ_{O2C}, of the reactants and the temperature of the CPOX catalyst bed, T_{cpox}. All reactions in the CPOX occur concurrently. However, to simplify the model, we view the overall CPOX reaction as a sequential process of Reactions (20)–(23), as illustrated in Fig. 4.

The figure notations is: r = "react", nr = "not react" and f = "from". The three main variables that define the calculation of CPOX conversion are α, S, and β. Their definitions are

$$\alpha := \frac{\text{Rate of } CH_4 \text{ reacts}}{\text{Rate of } CH_4 \text{ enters}}, \tag{24}$$

$$S := \frac{\text{Rate of } CH_4 \text{ reacting in POX}}{\text{Total rate of } CH_4 \text{ reacting}}, \tag{25}$$

$$\beta := \frac{\text{Rate of } O_2 \text{ reacts with } H_2}{\text{Rate of } O_2 \text{ reacts with both } H_2 \text{ and CO}}. \tag{26}$$

Variable α is a function of both T_{cpox} and λ_{O2C}, S is a function of λ_{O2C} and β is a constant. The expression of α is developed using curve fitting of the result in Zhu et al. (2001).

$$\alpha = \begin{cases} \alpha_1 \lambda_{O2C}, & \lambda_{O2C} < 0.5, \\ 1 - (1 - 0.5\alpha_1)(1 - \tanh(\alpha_2(\lambda_{O2C} - 0.5))), & \lambda_{O2C} \geqslant 0.5, \end{cases} \tag{27}$$

where $\alpha_1 = \min(2, 0.0029 T_{cpox} - 1.185)$ and $\alpha_2 = 0.215 e^{3.9 \times 10^{-8}(T_{cpox}-600)^3}$. The plot of α is shown in Fig. 5.

CH_4 reacts in either POX or TOX reactions depending on the initial O2C ratio, which, in this model, is the O2C ratio in the MIX. The difference between the rate of POX and TOX reaction is described by the selectivity, S. Here we assume that the function is linear, as shown in Fig. 6, which agrees with the results from the high-temperature thermodynamic equilibrium in (Zhu et al. (2001)). The relation between the selectivity and the O2C ratio in Fig. 6 can be expressed as

$$S = \begin{cases} 1, & \lambda_{O2C} < \frac{1}{2}, \\ \frac{2}{3}(2 - \lambda_{O2C}), & \frac{1}{2} \leqslant \lambda_{O2C} \leqslant 2, \\ 0, & \lambda_{O2C} > 2. \end{cases} \tag{28}$$

Values of S close to one indicate that more POX reaction takes place and thus more H_2 is generated. Since there are 2 mole of H_2 produced per one mole of CO produced in POX reaction, O_2 reacts with H_2 more than CO and, thus, the ratio β is kept constant at $\beta = \frac{2}{3}$.

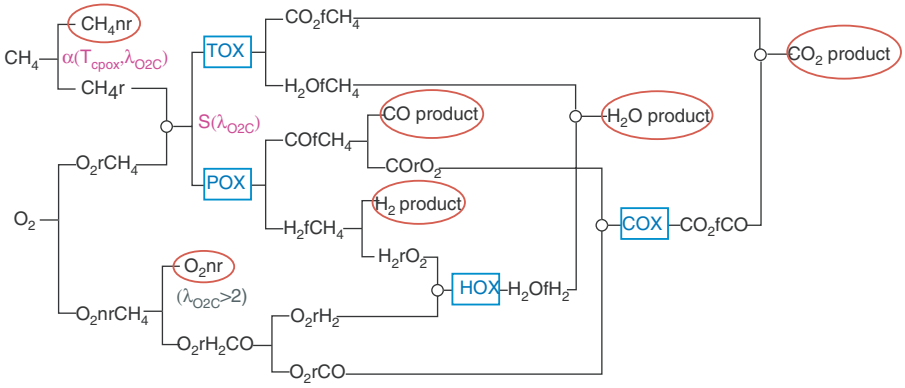

Fig. 4. Illustration of calculation of CPOX reactions.

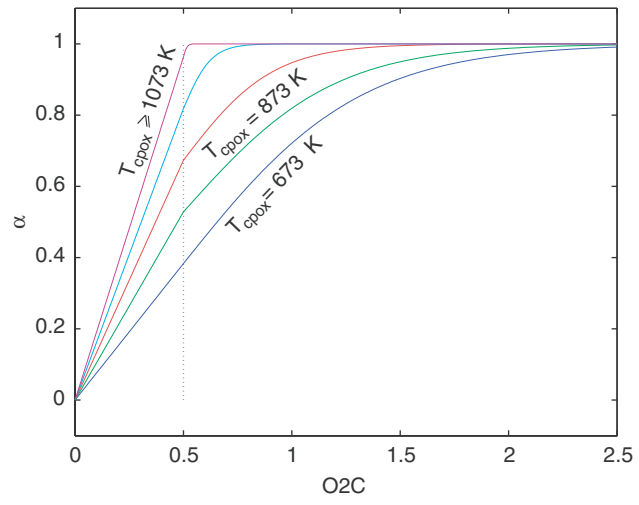

Fig. 5. Amount of CH_4 reacted as a function of T_{cpox} and λ_{O2C}.

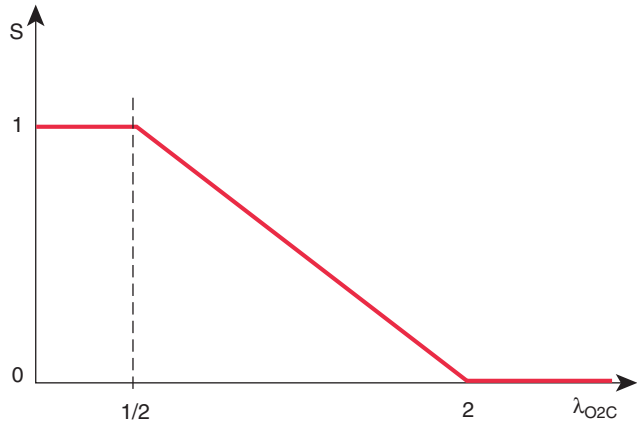

Fig. 6. Selectivity between POX and TOX.

As explained earlier, when $\lambda_{O2C} < \frac{1}{2}$, the supplied oxygen is not sufficient to oxidize all supplied fuel and the H_2 production rate is limited by the amount of oxygen. At normal operation, λ_{O2C} is kept higher than $\frac{1}{2}$ in order to avoid wasting the fuel. A high value of λ_{O2C} (low S) indicates that there is more TOX reaction. Since more heat is released from TOX reaction, operating CPOX at high λ_{O2C} will overheat the CPOX and can permanently damage the catalyst bed. The desired value of λ_{O2C} in the literature varies from 0.4 to 0.6 (Chan & Wang, 2000; Pino et al., 2002; Recupero, Pino, Leonardo, Lagana, & Maggio, 1998). In this study, the desired value is chosen at $\lambda_{O2C} = 0.6$ in order to allow some buffer for λ_{O2C} before it becomes lower than $\frac{1}{2}$ during transient deviations.

The calculation of the species in the CPOX model is calculated in mole basis. The molar flow rate of the gas entering the CPOX can be calculated from

$$N_{i,in} = \frac{x_i^{mix} W_{cpox}}{M_i}, \tag{29}$$

where i represents CH_4, O_2, N_2, and H_2O; M_i is the molecular mass of gas i; and W_{cpox} and x_i^{mix} are the CPOX total flow rate and mole fraction of gas i in MIX, both are calculated in the MIX model (Eqs. (13)–(17)). Following the diagram in Fig. 4, the set of equations to calculate the total product of CPOX reaction is given as

$$N_{H_2} = [2S\alpha - 2\beta(\lambda_{O2C} - \lambda_x\alpha)\text{sign}(S)]N_{CH_4in},$$

$$N_{CO} = [S\alpha - 2(1-\beta)(\lambda_{O2C} - \lambda_x\alpha)\text{sign}(S)]N_{CH_4in},$$

$$N_{CO_2} = [(1-S)\alpha + 2(1-\beta)(\lambda_{O2C} - \lambda_x\alpha)\text{sign}(S)]N_{CH_4in},$$

$$N_{H_2O} = [2(1-S)\alpha + 2\beta(\lambda_{O2C} - \lambda_x)\text{sign}(S)] \times N_{CH_4in} + N_{H_2Oin},$$

$$N_{CH_4} = (1-\alpha)N_{CH_4in},$$

$$N_{O_2} = (N_{O_2in} - \lambda_x\alpha N_{CH_4in})\text{sign}(S),$$

$$N_{N_2} = N_{N_2in}, \tag{30}$$

where $\lambda_x = (2 - \frac{3}{2}S)$. A plot of products calculated from (30), assuming no inlet N_2 and H_2O, is shown in Fig. 7, which matches with the theoretical results in Zhu et al. (2001). The mass flow rate of each species leaving the CPOX is $W_i^{cpox} = M_i N_i$. The mass conservation property of chemical reactions ensures that the total mass flow across the CPOX is conserved, i.e., $\sum W_i^{cpox} = W^{cpox}$.

The dynamic equation of temperature (19) can now be expanded. The enthalpy of the gas flow depends on the flow rate, the flow temperature, and the gas composition. Thus

$$\begin{bmatrix}\text{Enthalpy}\\ \text{flow in} - \text{out}\end{bmatrix} = W^{cpox}(C_P^{mix}(T_{mix} - T_{ref}) - C_P^{cpox}(T_{cpox} - T_{ref})), \tag{31}$$

where T_{ref} is the reference temperature (298 K). The gas specific heat C_P^{mix} and C_P^{cpox} (J/kg K) are that of the gas in the mixer (gas before CPOX reaction) and the gas in the CPOX (after reaction), respectively. They are functions of gas composition and gas temperature.

$$C_P^{mix} = \sum x_i^{mix} C_{P_i}(T_{mix}), \tag{32}$$

$$C_P^{mix} = \sum x_i^{cpox} C_{P_i}(T_{cpox}), \tag{33}$$

where i represents four species in the MIX (Eq. (29)) and seven species in the CPOX (Eq. (30)). The heat released from the reaction depends on the amount of reaction

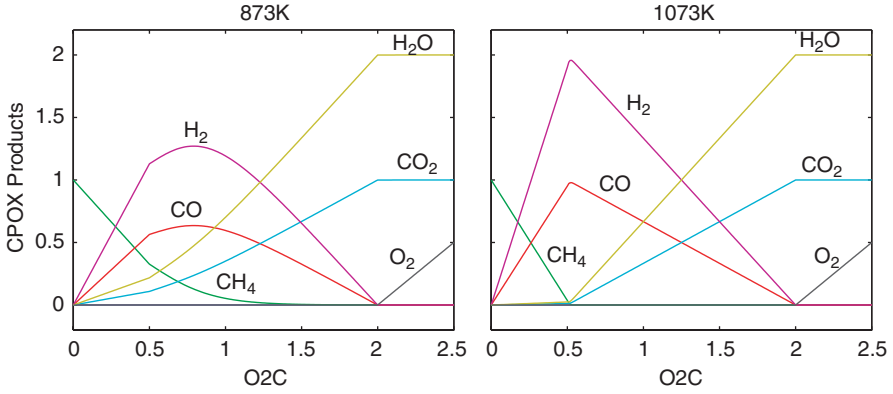

Fig. 7. Products of CPOX reaction per unit of CH_4 entering CPOX.

taking place.

$$\begin{bmatrix}\text{Heat}\\ \text{from}\\ \text{reaction}\end{bmatrix} = N_{CH_4 r}(S\cdot(-\Delta H^0_{pox}) + (1-S)\cdot(-\Delta H^0_{tox})) + N_{O_2 r H_2 CO}(\beta\cdot(-\Delta H^0_{hox}) + (1-\beta)\cdot(-\Delta H^0_{cox})), \quad (34)$$

where $-\Delta H^0_{pox}$, $-\Delta H^0_{tox}$, $-\Delta H^0_{hox}$, and $-\Delta H^0_{cox}$ (J/mol) are the heat released from POX, TOX, HOX, and COX reactions, respectively.

3.9. Water–gas shift converter and preferential oxidation reactor (WROX)

The WGS converter and the preferential oxidation reactor are lumped together as one volume, denoted as WROX. Three flows entering the volume are H_2-rich gas flow from the CPOX, W^{cpox}, water injection needed for WGS reaction, $W^{wgs}_{H_2O}$, and air injection required for PROX reaction, W^{prox}_{air}. The WROX model has two states, which are total pressure, p^{wrox}, and H_2 pressure, $p^{wrox}_{H_2}$. Since the amount of CO created in CPOX is proportional to the rate of H_2 created (POX reaction), it is assumed that the rate of H_2 generated in the WGS is a fixed percentage (η_{wrox}) of the rate of H_2 generated in the CPOX. The state equations are

$$\frac{dp^{wrox}}{dt} = \frac{RT_{wrox}}{M_{wrox}V_{wrox}}(W^{cpox} - W^{wrox} + W^{wgs}_{H_2O} + W^{prox}_{air}), \quad (35)$$

$$\frac{dp^{wrox}_{H_2}}{dt} = \frac{RT_{wrox}}{M_{H_2}V_{wrox}}((1+\eta_{wrox})W^{cpox}_{H_2} - x^{wrox}_{H_2}W^{wrox}), \quad (36)$$

where M_{wrox} is an average molecular weight of the gas in WROX, and T_{wrox} is an average temperature of WGSs and PROX. The WROX exit flow rate, W^{wrox}, is calculated using the nozzle (6) based on the pressure drop between WROX and anode volume, $p^{wrox} - p^{an}$. The H_2 mass fraction in WROX, $x^{wrox}_{H_2}$, can be determined from the two states by

$$x^{wrox}_{H_2} = \frac{M_{H_2}}{M_{wrox}}\frac{p^{wrox}_{H_2}}{p^{wrox}}. \quad (37)$$

The rate of water injected into WROX, $W^{wgs}_{H_2O}$, is equal to the amount that is required to cool the gas from CPOX down to the desired WGSs inlet temperatures (Brown, 2001; Doss et al., 2001). There are two WGS reactors and thus the total rate of water injected is $W^{wgs}_{H_2O} = W^{wgs1}_{H_2O} + W^{wgs1}_{H_2O}$. The flow rate of water into each WGS is calculated using energy balance between enthalpy of the gas flows, enthalpy of the flow at the desired temperature, and the heat of water vaporization. It is assumed that the PROX air injection, W^{prox}_{air}, is scheduled based on the stack current at the value twice needed (Brown, 2001; Doss et al., 2001) at the designed operating condition.

3.10. Anode

Mass conservation is used to model the pressure dynamics in the anode volume. To simplify the model, only three mass flows are considered, including flows into and out of the anode volume and the rate of H_2 consumed in the fuel cell reaction. The dynamic equations are

$$\frac{dp^{an}}{dt} = \frac{RT_{an}}{M_{an}V_{an}}(W^{wrox} - W^{an} - W_{H_2,react}), \quad (38)$$

$$\frac{dp^{an}_{H_2}}{dt} = \frac{RT_{an}}{M_{H_2}V_{an}}(x^{wrox}_{H_2}W^{wrox} - x^{an}_{H_2}W^{an} - W_{H_2,react}), \quad (39)$$

where W^{an} is calculated as a function of the anode pressure, p^{an}, and the ambient pressure, p_{amb}, using Eq. (6). We assume that the anode temperature and humidity are slowly varying and are approximately equal to the anode inlet flow temperature and humidity

(fully saturated flow), respectively. The rate of H_2 reacted is a function of stack current, I_{st}, through the electrochemistry principle (Larminie & Dicks, 2000)

$$W_{H_2,react} = M_{H_2}\frac{nI_{st}}{2F}, \tag{40}$$

where n is the number of fuel cells in the stack and F is the Faraday's number (96 485 C).

Two meaningful variables which are H_2 utilization, U_{H_2}, and anode H_2 mole fraction, y_{H_2}, can be calculated by

$$U_{H_2} = \frac{\text{H}_2 \text{ reacted}}{\text{H}_2 \text{ supplied}} = \frac{W_{H_2,react}}{x_{H_2}^{wrox} W^{wrox}} \tag{41}$$

and

$$y_{H_2} = \frac{p_{H_2}^{an}}{p^{an}}. \tag{42}$$

The H_2 utilization represents stack efficiency while the H_2 mole fraction is used as an indication of stack H_2 starvation. Low H_2 utilization means that more H_2 is wasted to the anode exhaust and thus the stack efficiency is low. High utilization represents to high fuel cell efficiency. However, it increase the risk of fuel cell H_2 starvation during transient.

4. Model integration, calibration, and verification

The low-order (10 states) model described in the previous sections is developed in MATLAB/Simulink platform. The model is parameterized and validated with the results of a high-order (>300 states) detailed model (Eborn et al., 2003) described in Section 5 instead of actual experiments on the physical system. The detailed model includes spatial variation and exact chemical reaction rates for all the species. The detailed model is developed using Dymola software (Tiller, 2001) and is imported as an S-function in Simulink. For validation purposes the outputs from the two models are compared with equivalent inputs in Section 6.

In a very aggressive development cycle, where (i) components, (ii) system design decisions, and (iii) control design occur concurrently, accessing transient experimental data is prohibitively expensive or even impossible. We thus use the complex system model described next as a benchmark of the real system behavior.

5. System level dynamic model of fuel cell system

Fuel cell systems are truly heterogeneous systems involving mechanical, chemical, thermal and electrical systems. They also contain a complex flow network near ambient pressure with several recycle flows and strong couplings between subsystems. Having a model team working concurrently on system models consisting of hundreds of components, several hundred dynamic states and more than 20 000 equations is a very complex task. This puts strict requirements on model library structure and version control. Moreover, the model libraries need to accommodate typically the needs of several teams such as stationary and automotive applications. All these requirements make system level modeling a significant challenge that very few modeling tools can handle (Åström & Bell, 2000).

Modelica/Dymola is a domain-independent language with many capabilities and emphasis in system dynamics that has been used for the more detailed, physics-based model of fuel cell systems at United Technologies Corporation (UTC). Modelica is an equation-based, object-oriented language for physical systems modeling (Tiller, 2001). Modelica has been developed as an open standard and intended for multi-domain, heterogeneous systems. Reusable component models are described in Modelica using hybrid, differential–algebraic equations. Complex system models can be assembled using the component models. Dymola is a commercial development/simulation environment for Modelica. The model library is based on the ThermoFluid library, which is an open source model library. Here, we describe briefly the detailed physics-based Dymola model used for validating the simplified model presented in this paper.

Besides the FPS, described in Section 2, the Modelica fuel cell system model includes the cell stack assembly (CSA), power conditioning system (PCS) and the thermal management system (TMS) to emulate realistic responses that allow us to focus on the H_2 generation problem. For example the Modelica model includes the thermal management system (TMS) in order to ensure good humidity and temperature condition in the anode

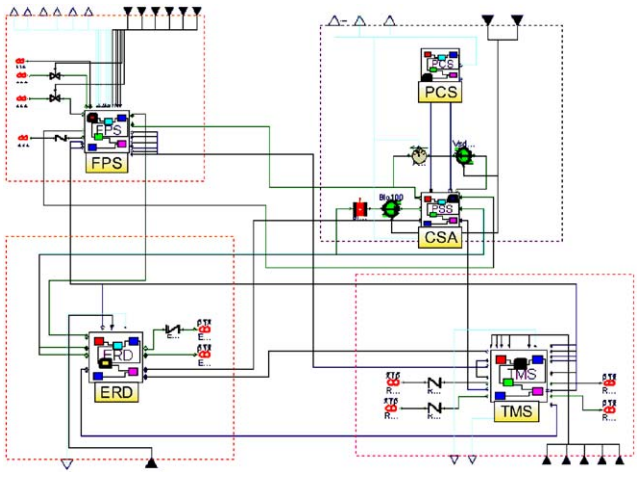

Fig. 8. Fuel cell system level model in Dymola, including FPS, CSA, PCS and TMS.

of the CSA. A diagram of the system in Dymola is shown in Fig. 8, all lines between subsystems are physical connections carrying information on pressure, flows and composition. The triangular connectors at the outside of the diagram are control inputs and measured outputs.

The FPS and CSA are the most complex subsystems. The FPS comprises detailed models of all the previously described reaction stages; CPOX, two WGS and two PROX reactors. The reactor models are described as continuous stirred tanks (CSTR) and employ bulk rate expressions based on experimental data. Besides the oxidation reactions for CH_4 and H_2, CO is included in the simplified model. Additional detailed reactions are also included in the CPOX model

$$CH_4 + H_2O \leftrightarrow CO + 3H_2 \quad \text{(steam reforming)},$$

$$CO + H_2O \leftrightarrow CO_2 + H_2 \quad \text{(water}-\text{gas shift)}$$

that describe the exact flow composition and temperature. The oxidation reactions assume oxygen mass transfer limitation while the steam reforming and WGS are equilibrium reactions. The two WGS reactors model the equilibrium-limited shift reaction and operate at different temperatures. The two PROX reactors model CO and H_2 oxidation reactions and also operate at different temperatures. These exact reaction rates and energy equations establish a wide range of fidelity but introduce a large complexity. Note here that the simplified model is based on well-controlled (constant and nominal) conditions in the WGS and the PROX that allow us to lump them in one volume equation (WROX) (35).

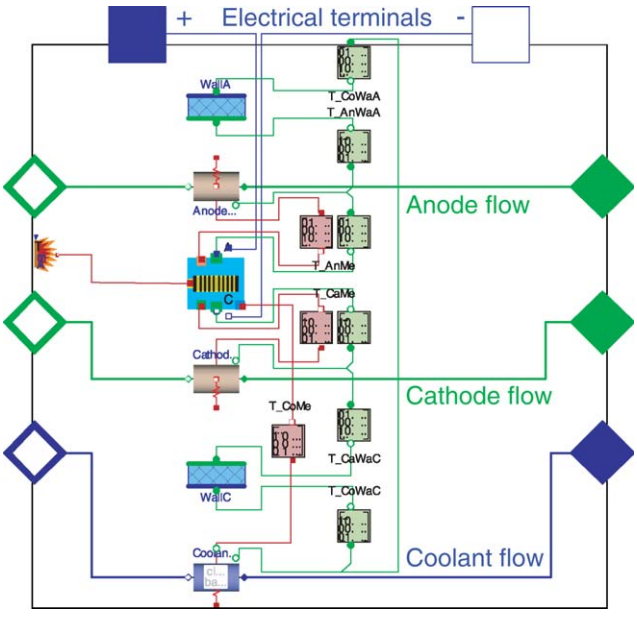

Fig. 9. Cell stack model diagram, showing the split into volume models for anode, cathode and coolant flow fields and membrane models inbetween describing diffusion of gases and liquids.

The cell stack model is shown in Fig. 9. It is a very good example of how public model libraries can be used to build proprietary component models. All the flow-fields are described by general volume models from the ThermoFluid library, which include the basic balance equations and ideal gas medium models. The volumes are discretized with multi-node approximations and separated with membrane models that incorporate gas and liquid diffusion. The membrane models are proprietary, as well as the connection matrices that describe the flow field layout and the voltage–current characteristic, which is included in the membrane model.

Also the reactor models are based on volumes from the ThermoFluid library. The multi-node configuration (train of CSTR's) has been used to approximate one-dimensional distributed systems. Due to the object-oriented features, ThermoFluid allows different choices for state variables in the resulting differential equation system without having to rewrite the component models. We have used the pressure, temperature and mass fractions (p, T, x) formulation as well as the component mass and temperature (M_i, T) formulations. The choice of state variables affects the numerical properties of the model since the coordinate transformation is nonlinear.

The Dymola power plant model is interfaced with the controller description in Simulink. The controller consists of both the sequential control logic as well as the continuous process control loops that track any load changes during operation. For the purpose of validation of the simplified model, the fuel and air actuator inputs to the open loop plant model have been perturbed around the design operating point.

The system level model is used in all the design stages of the fuel cell development process at UTC. Feasibility and limits of performance of different designs are tested in the conceptual design phase, the sequential control that takes the plant through startup and shutdown is implemented in StateFlow and tested in the preliminary design phase. In the final, critical design, the continuous controls are implemented and tuned to verify the controller structure against the dynamic requirements such as load following capability over the entire operating range. However, the complexity of the system level model makes it impractical to use for systematic, multi-variable control design. For hardware-in-the-loop applications linearized models at different operating points have been used, but the full system model with more than 500 states needs to be reduced to around 50 states for real-time simulation. Even with this size of model most modern control synthesis methods will have numerical limitations that make them impractical to use. Thus there is a need for the bottom-up control-oriented modeling approach described in this article. Simplified, physical models can be used both for observer design (Arcak, Gorgun, Pedersen, & Varigonda, 2004) and controls analysis and design (Pukrushpan et al., 2005).

Table 3
Typical model parameters for a 200 kW system

Parameter	Typical value
T_{hex}	400–500 K
V_{hex}	0.05 m^3
$W_{0,hex}$	0.04 kg/s
$\Delta p_{0,hex}$	450–500 Pa
T_{hds}	350–400 °C
V_{hds}	0.3 m^3
p_{tank}	133 kPa
$W_{0,valve}$	0.0075 kg/s
$\Delta p_{0,valve}$	3600 Pa
$W_{0,hds}$	0.0075 kg/s
$\Delta p_{0,hds}$	100–110 Pa
T_{mix}	300 °C
V_{mix}	0.03 m^3
$C_{P,bed}^{cpox}$	450 J/kg K
m_{bed}^{cpox}	2.8 kg
$W_{0,cpox}$	0.05 kg/s
$\Delta p_{0,cpox}$	3000 Pa
η_{wrox}	20–50 %
T_{wrox}	500 K
V_{wrox}	0.45 m^3
M_{wrox}	16×10^{-3} kg/mol
$T_{wgs1,in}^{des}$	400 °C
$T_{wgs2,in}^{des}$	200 °C
T_{wgs1}	400 °C
$W_{0,wrox}$	0.06 kg/s
$\Delta p_{0,wrox}$	2000 Pa
T_{an}	65–80 °C
V_{an}	0.0045 m^3
M_{an}	27.8×10^{-3} kg/mol
n	750–1000 Cells
$W_{0,an}$	0.06 kg/s
$\Delta p_{0,an}$	500–600 Pa

[Brown, 2001, de Smet et al., 2001, Dicks, 1996, Recupero et al., 1998]

6. Simulation and model validation

The model parameters for a system designed to be used for residential or commercial buildings are given in Table 3. Similar power range would be needed for a bus or a heavy-duty vehicle propulsion system. The focus of our work is to capture the essential dynamic input/output behavior, and, thus our main focus is reasonable agreement of transient responses. The FPS key performance variables are the O2C ratio, the CPOX temperature, the FPS exit total flow rate, and the FPS exit H_2 flow rate. Several parameters, such as the orifice constants and the component volumes, are adjusted appropriately in order to obtain comparable transient responses. Note that the model is expected to provide a close prediction of the transient response of the variables located upstream of the WGS inlet (WROX inlet). On the other hand, a relatively large discrepancy is expected for the variables downstream from the CPOX since the WGS and PROX reactors are approximately modeled as one lumped volume and are assumed perfectly controlled, which is not the case for the Dymola model.

The nominal operating point used in the validation is chosen at the O2C ratio $\lambda_{O2C} = 0.6$ and the stack H_2 utilization $U_{H_2} = 80\%$ (Doss et al., 2001). Step changes (up/down) of the three inputs: the stack current, I_{st}, the blower signal, u_{blo}, and the fuel valve signal, u_{valve}, are applied individually at time 400, 800, and 1200 s, respectively, followed by the simultaneous step changes of all inputs at 1600 s. The responses of the key variables are shown in Fig. 10. In the right column is the zoom-in of the response at 1600 s which represents the simultaneous input step increase.

At 400 s where the step of stack current is applied, the low-order model does not show any transient since the stack current only affects the H_2 consumption in the anode which has very little influence on the FPS variables. On the other hand, the high-order model shows small transient. This transient is caused by a build-in feedforward controller in the high-order model, that adjusts several flow rates based on the changes in stack current. The feedforward controller is not implemented in the low-order model.

The step of air blower command at 800 s raises CPOX temperature, which is a result of an increase in O_2-to-CH_4 ratio. Since O_2 to CH_4 ratio rises, the rate of POX reaction decreases, thus lowers the final product H_2, as shown in the response of $W_{H_2,fps}$. However, there is an initial increase of $W_{H_2,fps}$ right at 400 s that is caused by the increase of total flow that initially has high H_2 concentration. This behavior indicates that the FPS plant has non-minimum phase (NMP) relation from the blower command to the H_2 generation. This NMP response can also be observed when blower command decreases, as seen from $W_{H_2,fps}$ response at 1000 s.

During the step increase in fuel valve command (at 1200 s), the O_2-to-CH_4 ratio drops and results in more POX reaction, thus more H_2 is generated ($W_{H_2,fps}$ increases). After the initial increase in $W_{H_2,fps}$, TOX reaction drops and heat generated from the reaction is not sufficient to maintain the CPOX temperature. The drop in T_{cpox} later lower the rate of CH_4 reacts (see Fig. 5), thus, reduce the product H_2, i.e. $W_{H_2,fps}$ decrease.

It can be seen that, despite the offset, there is a good agreement between the two models for most transient responses. The model is also tested at different power (current) operations and transient responses also agree well. A more accurate model can be developed with the expense of extra complexity and/or higher system order.

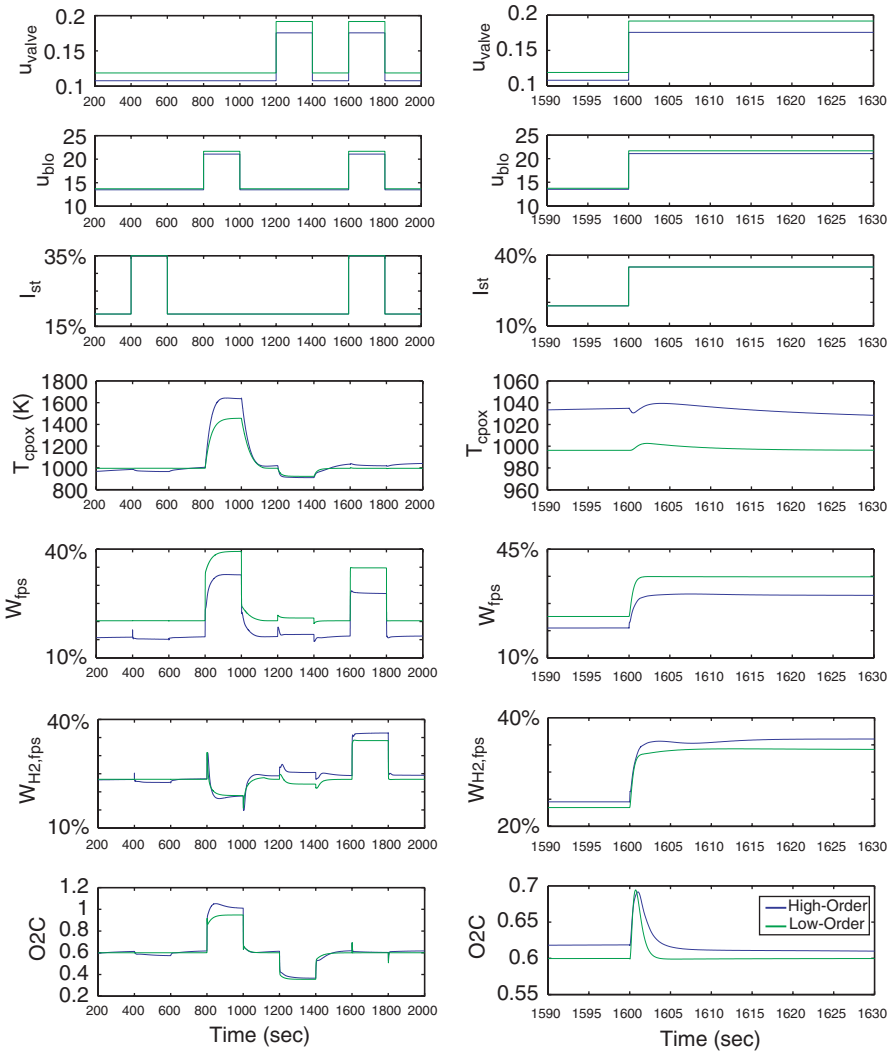

Fig. 10. Model validation results: inputs and performance variables. Blue (Dark) = high-order model; green (light) = low-order model.

7. Model applications

The dynamic FPS model is useful for control analysis and design. It can be used to investigate potential subsystem conflicts. It accounts for nonlinear interactions between subsystems and it can be augmented with constraints from sensor fidelity or actuator authority. Here, we illustrate two control-related applications of the model. First, the model is used in a multivariable analysis to determine characteristics of the system that might limit performance of a controller or a control configuration. Second, the model can be used to develop real-time observers to estimate critical stack variables that may be hard to measure or augment existing stack sensors for redundancy in fault detection (Glass, 2000).

In Section 7.1, a control problem is formulated by means of defining control input, performance variables and potential measurements. Section 7.2 illustrates the use of the RGA analysis to determine control input/output pairs and to identify the interactions between two control loops. Section 7.3 presents an observability analysis of the model that is useful in selecting measurements.

7.1. Control problem formulation

As previously discussed, one of the key requirements of the FPS controller are to quickly replenish the H_2 that is consumed in the fuel cell anode during current (load) changes. On the other hand, the FPS controller needs to reduce the H_2 generation when there is a step-down in the current drawn from the fuel cell so H_2 is not wasted. This H_2 on demand operation involves the following objectives (i) to protect the stack from damage due to H_2 starvation (ii) to protect CPOX from overheating and (iii) to keep overall system efficiency high, which includes high stack H_2 utilization and high FPS CH_4-to-H_2 conversion. Objectives (i) and (ii) are important during transient operations while objective

(iii) can be viewed as a steady-state goal. Objectives (ii) and (iii) are also related since maintaining the desired CPOX temperature during steady-state implies proper regulation of the (O2C) ratio which corresponds to high FPS conversion efficiency.

In the following study, we ignore the effect of temperature on the CH_4 reaction rate which equivalent to assuming that all CH_4 that enters the CPOX reacts. Note that these assumptions reduce the validity of the model for large T_{cpox} deviations. However, achieving one of the control goals, which is the regulation of T_{cpox}, will ensure that this modeling error remains small.

The desired steady-state is selected at stack H_2 utilization $U_{H_2} = 80\%$ (Doss et al., 2001) and CPOX (O2C) ratio $\lambda_{O2C} = 0.6$. With this specification, the model gives the value of CPOX temperature, $T_{cpox} = 972\,\mathrm{K}$ (corresponds to $\lambda_{O2C} = 0.6$), and the value of anode H_2 mole fraction, $y^{an}_{H_2} \approx 8\%$ (corresponds to $U_{H_2} = 80\%$). The control objective is therefore to regulate T_{cpox} at 972 K and $y^{an}_{H_2}$ at 0.08. This desired value of $T_{cpox} = 972\,\mathrm{K}$ also agrees with the value published in the literature (de Smet, de Croon, Berger, Marin, & Schouten, 2001).

High T_{cpox} can cause the catalyst bed to overheat and be permanently damaged. Low T_{cpox} results in a low CH_4 reaction rate in the CPOX (Zhu et al., 2001). Large deviations of $y^{an}_{H_2}$ are undesirable. On one hand, a low value of $y^{an}_{H_2}$ means anode H_2 starvation (Song et al., 2000; Springer, Rockward, Zawodzinski, & Gottesfeld, 2001) which can permanently damage the fuel cell structure. On the other hand, a high value of $y^{an}_{H_2}$ means small H_2 utilization which results in a waste of H_2.

The stack current, I_{st}, is considered as an exogenous input that is measured. Since the exogenous input is measured, we consider a two degrees of freedom (2DOF) controller based on feedforward and feedback, as shown in Fig. 11. The control problem is formulated using the general control configuration shown in Fig. 12. The two control inputs, u, are the air blower signal, u_{blo}, and the fuel valve signal, u_{valve}. The feedforward terms that provide the valve and the blower signals that reject the steady-state effect of current to the outputs are

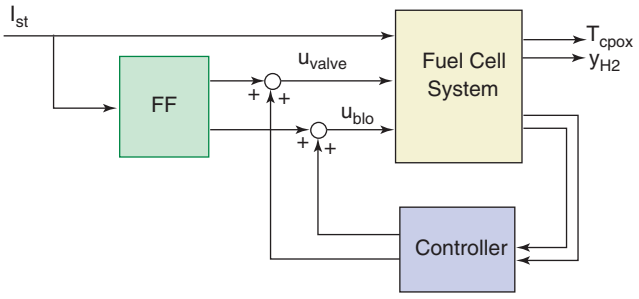

Fig. 11. Feedback control study.

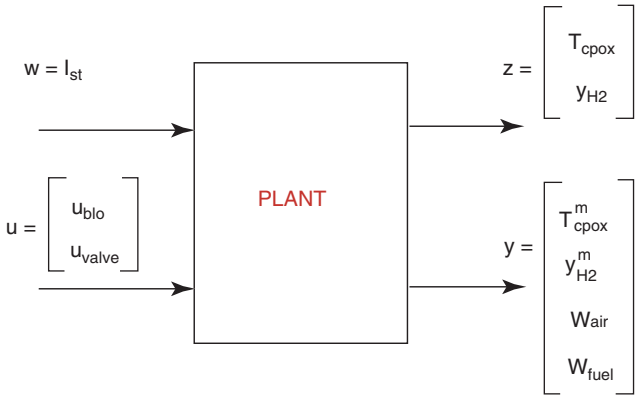

Fig. 12. Control problem.

integrated in the plant:

$$u^* = \begin{bmatrix} u^*_{blo} \\ u^*_{valve} \end{bmatrix} = f_I(I_{st}). \tag{43}$$

The value of u^* is obtained by the nonlinear simulation and can be implemented with a lookup table. The performance variable, z, includes the CPOX temperature, T_{cpox}, and the anode exit H_2 mole fraction, $y^{an}_{H_2}$. The system represents a two-input two-output (TITO) system when viewed from the inputs, u, to the performance variables, z.

Several sets of measured variables are considered. The variables that can be potentially measured are the CPOX temperature, T^m_{cpox}, the H_2 mole fraction, $y^m_{H_2}$, the air flow rate through the blower, W_{air}, and the fuel flow rate, W_{fuel}. The measured values, T^m_{cpox} and $y^m_{H_2}$, are the values obtained from realistic sensors, which has measurement lag. The control objective is to reject or attenuate the response of z to the disturbance w by controlling the input, u, based on the measurement, y.

7.2. Input–output pairing and loop interactions

One of the most common approaches to controlling a TITO system is to use a diagonal controller, which is often referred to as a decentralized controller. The decentralized control works well if the plant is close to diagonal which means that the plant can be considered as a collection of individual single-input single-output (SISO) sub-plants with no interaction among them. In this case, the controller for each sub-plant can be designed independently. If an off-diagonal element is large, then the performance of the decentralized controller may be poor.

A linear model of the FPS is obtained by linearizing the nonlinear model. The operating point is set at $\lambda_{O2C} = 0.6$ and $U_{H_2} = 0.8$ and static feedforward terms (illustrated in Fig. 11) are included in the linear plant. The

linearization of the plant is denoted by

$$\Delta\dot{x} = A\Delta x + B_u\Delta u + B_w\Delta w,$$

$$\Delta z = C_z\Delta x + D_{zu}\Delta u + D_{zw}\Delta w,$$

where the state, x, input, u, disturbance, w, and performance variables, z, are

$$x = \left[T_{cpox}\ p^{an}_{H_2}\ p^{an}\ p^{hex}\ \omega_{blo}\ p^{hds}\ p^{mix}_{CH_4}\ p^{mix}_{air}\ p^{wrox}_{H_2}\ p^{wrox}\right]^{\mathrm{T}}$$

$$w = I_{st}, \quad u = [u_{blo}\ u_{valve}]^{\mathrm{T}}, \quad z = \left[T_{cpox}\ y^{an}_{H_2}\right]^{\mathrm{T}}.$$

For simplicity, the symbol Δ, which denotes the deviation of the variables from the nominal point, will be dropped for the rest of the paper. The current input is in Ampere. The blower and the valve signals, u_{blo} and u_{valve}, vary between 0 and 100. The outputs are the CPOX temperature in Kelvin and the anode H_2 mole fraction in percent. In the transfer function form, we can represent the plant as

$$z = G\begin{bmatrix} w \\ u \end{bmatrix} = \begin{bmatrix} G_{zw} & G_{zu} \end{bmatrix}\begin{bmatrix} w \\ u \end{bmatrix}. \tag{44}$$

Different linear models can be obtained by linearizing the nonlinear plant model at different operating conditions, for example, different current (load) levels, 30%, 50%, and 80%. Each linear model represents the behavior of the nonlinear plant close to the operating condition used.

The open-loop response of the linear system is shown in Fig. 13. The output are in the units as follows: $y^{an}_{H_2}$ (%) and T_{cpox} (K). For clarity, in these two figures, the units of current is (decaAmp $= \times 10$ A).

Note first that the feedforward controller does well in rejecting the effect from I_{st} to y_{H_2} and U_{H_2} in steady state. The steady-state cancellation is perfect at the 50% load because the feedforward terms have been designed for the 50% load. The feedforward H_2 starvation recovers, however, relatively slow. A feedback controller is, thus, needed to speed up the system behavior and reduce the sensitivity introduced by modeling uncertainty.

The responses of the output due to step changes in the actuator signals show a strongly coupled system. The fuel dynamics are slower than the air dynamics, primarily due to the large HDS volume. Unfortunately, the fast air dynamics cannot be used effectively to improve starvation because of the non-minimum phase behavior observed between the blower input u_{blo} to anode H_2 mole fraction. Thus, fast fuel dynamics are important for improving the H_2 generation response of the FPS system. On the other hand, good temperature regulation might benefit from the coordination of the two actuators.

A method used to measure the interaction between the two loops and assess appropriate pairing and

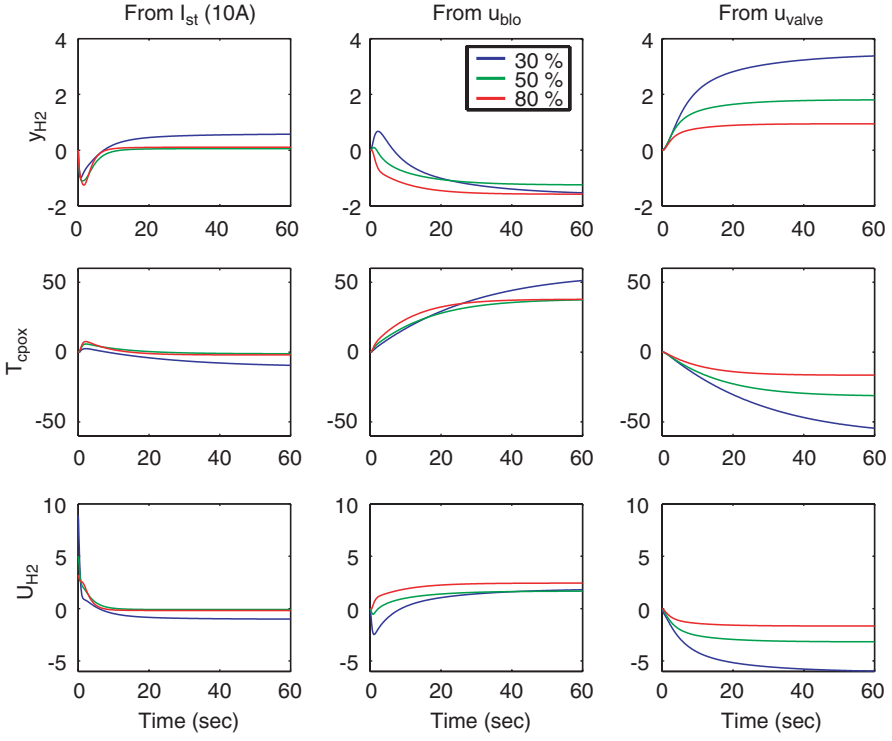

Fig. 13. Step responses of linearized models at 30%, 50% and 80% power.

controller architecture is called Relative Gain Array (RGA) (Bristol, 1966). The RGA is a complex non-singular square matrix defined as

$$RGA(G) = G \times (G^{-1})^{\mathrm{T}}, \tag{45}$$

where $\times$ denotes element by element multiplication. Each element of RGA matrix indicates the interaction between the corresponding input–output pair. It is preferred to have a pairing that give RGA matrix close to identity matrix. The useful rules for pairing are (Skogestad & Postlethwaite, 1996)

1. To avoid instability caused by interactions at low frequencies one should *avoid* pairings with negative steady-state RGA elements.
2. To avoid instability caused by interactions in the crossover region one should *prefer* pairings for which the RGA matrix in this frequency range is close to identity.

The RGA matrices of G_{zu} of 50% system at steady-state is given in (46). According to the first rule, it is clear that the preferred pairing choice is $u_{blo} \rightarrow T_{cpox}$ pair and $u_{valve} \rightarrow y_{H_2}$ pair to avoid instability at low frequencies.

$$RGA(0 \text{ rad/s}) = \begin{bmatrix} 2.302 & -1.302 \\ -1.302 & 2.302 \end{bmatrix}. \tag{46}$$

However, it can be seen that at high frequencies, the diagonal and off-diagonal elements are closer which indicates more interactions. In fact, the plot of the difference between the diagonal and off-diagonal elements of RGA matrices of the linearized systems at 30%, 50% and 80% power in Fig. 14 shows that the interactions increase at high frequency. At low power level, the value of the off-diagonal element of RGA matrix is even higher than the diagonal element ($RGA_{11} - RGA_{12} < 0$) indicates large coupling in the system. At these frequencies, we can expect poor performance from a decentralized controller.

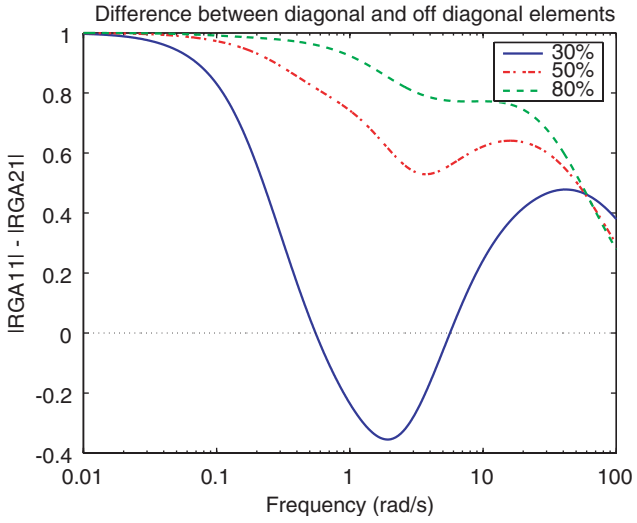

Fig. 14. Difference between diagonal and off-diagonal elements of the RGA matrix at different frequencies for three power setpoints.

Consequently, one should expect that fast controllers cannot be used for both loops because the control performance starts deteriorating due to system interactions. Moreover, since the interaction is larger for the low power (30%) system, the performance of fast decentralized control deteriorates significantly and can even destabilize the system. To prevent the deteriorating effect of the interactions, it is possible to design the two controllers to have different bandwidth. Therefore, to get fast y_{H_2} response while avoiding the effect of the interactions, the T_{cpox}-air loop needs to be slow. This compromise is not necessary for a multivariable controller that coordinates both actuators based on the errors in both performance variables. The analysis in this section suggests the need for multivariable control design (Pukrushpan et al., 2005).

7.3. Effect of measurements

The plant states can be estimated using the dynamic model of the plant together with available measurements. The observer state equations are

$$\dot{\hat{x}} = A\hat{x} + B_u u + B_w w + L(y - \hat{y}),$$

$$\hat{y} = C_y \hat{x} + D_{yu} u + D_{yw} w, \tag{47}$$

where $\hat{x}$ is the estimator state vector and L is the estimator gain. Different set of measurements, y, can be chosen.

The observability gramian, Q_{obs}, i.e. solution of

$$A^{\mathrm{T}} Q_{obs} + Q_{obs} A = -C_y^{\mathrm{T}} C_y, \tag{48}$$

is a tool to determine the degree of system observability for a set of measurements. If the gramian has full rank, the system is observable. However, a high condition number of the observability gramian indicates weak observability. Sometimes, this result arises because of poor selection of units of the model states (scaling). Thus, to better evaluate system observability, we normalize the condition number of the observability gramian (c_{obs}^N) by the value when all the states are measured, $y = x$ or $C_y = I$. For example, the normalized observability gramian when the two performance variables are measured is

$$c_{obs}^N = \frac{\text{cond}\,(Q_{obs,\{y=[T_{cpox}, y_{H_2}]\}})}{\text{cond}\,(Q_{obs,\{y=x\}})} = 2 \times 10^5. \tag{49}$$

Large normalized observability gramian implies that the system with perfect measurements of T_{cpox} and y_{H_2} is

Table 4
Normalized condition number of observability gramian

Measurements	Condition number
T_{cpox}, y_{H_2}	2×10^5
T^m_{cpox}, $y^m_{H_2}$	1.3×10^{10}
T^m_{cpox}, $y^m_{H_2}$, W_{air}, W_{fuel}	3672.7
T^m_{cpox}, $y^m_{H_2}$, W_{air}, W_{fuel}, p^{mix}	1928.8

weakly observable. In practice, the CPOX temperature measurement and anode H_2 mole fraction cannot be instantaneously measured. The temperature and H_2 sensors are normally slow, with time constants of approximately 40 and 10 s (The Argus Group, 2001), respectively. To assess the observability degradation for the realistic measurements, we augment the FPS dynamics with two additional states:

$$\begin{bmatrix} \dot{s_T} \\ \dot{s_H} \end{bmatrix} = \begin{bmatrix} -0.025 & 0 \\ 0 & -0.01 \end{bmatrix} \begin{bmatrix} s_T \\ s_H \end{bmatrix} + \begin{bmatrix} 0.025 & 0 \\ 0 & 0.01 \end{bmatrix} \begin{bmatrix} T_{cpox} \\ y_{H_2} \end{bmatrix}, \quad (50)$$

where S_T is the CPOX temperature sensor state and S_H is the H_2 sensor state. The normalized observability gramian is then calculated to be 1.3×10^{10} as can be seen in Table 4. The lag in the measurements can potentially degrade the estimator performance, and thus the feedback bandwidth must be detuned in favor of robustness.

However, adding the fuel and air flow measurements lowers the observability condition number to a value lower than the one obtained with perfect measurement of T_{cpox} and y_{H_2}. We can, thus, expect a better estimation performance. Even better estimation can be expected if additional measurements such as mixer pressure are available, as shown in the table below. More work is needed to define the critical measurements that will be beneficial for the observer-based controller.

8. Conclusion

A low-order (10 states) nonlinear model of the FPS is developed with a focus on the dynamic behaviors associated with the flow and the pressures in the FPS, the temperature of the CPOX and the H_2 generation for a fuel cell. The model is based on physical parameters of the plant and can be easily scaled to represent any POX-based FPS. The FPS model is parameterized and validated against a high-order (>300 states) fuel cell system model, which was validated against experimental data. The transient behavior of the low-order model agrees well with that of the high-order model.

We show two case studies of how the model can facilitate multivariable dynamic analysis. First, the model is used to determine loop interactions that might limit the performance of a decentralized control configuration. Then, we present observability analysis that can help in measurement/sensor selection.

Acknowledgements

J.T. Pukrushpan and A.G. Stefanopoulou wish to acknowledge funding support from the National Science Foundation under Contract NSF-CMS-0201332 and Automotive Research Center (ARC) Contract DAAE07-98-3-0022. The authors would like to thank Thordur Runolfsson, Lars Pedersen, Scott Bortoff and Shubhro Ghosh at the United Technology Research Center and Huei Peng at the University of Michigan for their help and valuable comments.

References

Ahmed, S., & Krumpelt, M. (2001). Hydrogen from hydrocarbon fuels for fuel cells. *International Journal of Hydrogen Energy*, *26*, 291–301.

Arcak, M., Gorgun, H., Pedersen, L. M., & Varigonda, S. (2004). A nonlinear observer design for fuel cell hydrogen estimation. *IEEE Transactions on Control System Technology*, *12*(1), 101–110.

Åström, K. J., & Bell, R. D. (2000). Drum boiler dynamics. *Automatica*, *36*, 363–378.

Birch, S. (2001). Ford's focus on the fuel cell. *Automotive Engineering International*, 25–28.

Boyce, M. P. (1982). *Gas turbine engineering handbook*. Houston, TX: Gulf Publishing.

Bristol, E. H. (1966). On a new measure of interactions for multivariable process control. *IEEE Transactions on Automatic Control*, *AC-11*, 133–134.

Brown, L. F. (2001). A comparative study of fuels for on-board hydrogen production for fuel-cell-powered automobiles. *International Journal of Hydrogen Energy*, *26*, 381–397.

Chan, S. H., & Wang, H. M. (2000). Thermodynamic analysis of natural-gas fuel processing for fuel cell applications. *International Journal of Hydrogen Energy*, *25*, 441–449.

de Smet, C. R. H., de Croon, M. H. J. M., Berger, R. J., Marin, G. B., & Schouten, J. C. (2001). Design of adiabatic fixed-bed reactors for the partial oxidation of methane to synthesis gas: Application to production of methanol and hydrogen-for-fuel-cells. *Chemical Engineering Science*, *56*, 4849–4861.

Dicks, A. L. (1996). Hydrogen generation from natural gas for the fuel cell systems of tomorrow. *Journal of Power Sources*, *61*, 113–124.

Doss, E. D., Kumar, R., Ahluwalia, R. K., & Krumpelt, M. (2001). Fuel processors for automotive fuel cell systems: A parametric analysis. *Journal of Power Sources*, *102*, 1–15.

Eborn, J., Pedersen, L.M., Haugstetter, C., & Ghosh, S., (2003). System level dynamic modeling of fuel cell power plants. *Proceedings of the 2003 American control conference*. pp. 2024–2029.

Gardner, T. H., Berry, D. A., Lyons, K. D., Beer, S. K., & Freed, A. D. (2002). Fuel processor integrated H_2S catalytic partial oxidation

technology for sulfur removal in fuel cell power plants. *Fuel*, *81*, 2157–2166.

Glass, R.S., (2000). *Sensor needs and requirements for proton exchange membrane fuel cell systems and direct-injection engines*. Technical report, Department of Energy, April 2000. Published by Lawrence Livermore National Laboratory.

The Argus Group (2001). *Hydrogen sensor for automotive fuel cells from the Argus Group*. http://www.fuelcellsensor.com/.

Larentis, A. L., de Resende, N. S., Salim, V. M. M., & Pinto, J. C. (2001). Modeling and optimization of the combined carbon dioxide reforming and partial oxidation of natural gas. *Applied Catalysis*, *215*, 211–224.

Larminie, J., & Dicks, A. (2000). *Fuel cell systems explained*. West Sussex; England: Wiley.

Ledjeff-Hey, K., Roses, J., & Wolters, R. (2000). CO_2-scrubbing and methanation as purification system for PEFC. *Journal of Power Sources*, *86*, 556–561.

Pino, L., Recupero, V., Beninati, S., Shukla, A. K., Hegde, M. S., & Bera, P. (2002). Catalytic partial-oxidation of methane on a ceria-supported platinum catalyst for application in fuel cell electric vehicles. *Applied Catalysis A: General*, *225*, 63–75.

Pukrushpan, J. T., Stefanopoulou, A. G., & Peng, H. (2004). Control of fuel cell breathing. *IEEE Control System Magazines*, *24*(2), 30–46.

Pukrushpan, J. T., Stefanopoulou, A. G., Varigonda, S., Pedersen, L. M., Ghosh, S., & Peng, H. (2005). Control of natural gas catalytic partial oxidation for hydrogen generation in fuel cell applications. *IEEE Transactions on Control System Technology*, *13*(1), 3–14.

Recupero, V., Pino, L., Leonardo, R. D., Lagana, M., & Maggio, G. (1998). Hydrogen generator, via catalytic partial oxidation of methane for fuel cells. *Journal of Power Sources*, *71*, 208–214.

Skogestad, S., & Postlethwaite, I. (1996). *Multivariable feedback control: Analysis and design*. New York: Wiley.

Song, R.-H., Kim, C.-S., & Shin, D. R. (2000). Effects of flow rate and starvation of reactant gases on the performance of phosphoric acid fuel cells. *Journal of Power Sources*, *86*, 289–293.

Springer, T. E., Rockward, R., Zawodzinski, T. A., & Gottesfeld, S. (2001). Model for polymer electrolyte fuel cell operation on reformate feed. *Journal of The Electrochemical Society*, *148*, A11–A23.

Thomas, E., James, B. D., Lomax, F. D., Jr., & Kuhn, I. F., Jr. (2000). Fuel options for the fuel cell vehicle: Hydrogen, methanol or gasoline. *International Journal of Hydrogen Energy*, *25*, 551–567.

Tiller, M. (2001). *Introduction to physical modeling with modelica*. Boston: Kluwer Academic Publishers.

Yang, W.-C., Bates, B., Fletcher, N., & Pow, R. (1998). Control challenges and methodologies in fuel cell vehicle development. *SAE Paper 98C054*.

Zhu, J., Zhang, D., & King, K. D. (2001). Reforming of CH_4 by partial oxidation: Thermodynamic and kinetic analyses. *Fuel*, *80*, 899–905.